RSC Advances

ROYAL SOCIETY OF CHEMISTRY

www.rsc.org/advances

Enhanced Dielectric Properties of Acrylic Resin Elastomer based Nanocomposite with Thermally Reduced Graphene Nanosheets

Gaoqiang WANG, Jingwen WANG*, Shuwei ZHOU, Senqiang WU

Abstract: Acrylic resin elastomer (ARE) has drawn considerable attention in recent years due to its excellent film-forming property, flexibility and elasticity. However, low dielectric constant restricts its application. In this work, an ARE based composite material with enhanced dielectric properties was obtained via adding graphene nanosheets prepared by thermal reduction (TrGN) to the ARE (ARE/TrGN). Furthermore, Polyvinylpyrrolidone (PVP) has been used to improve the dispersibility of TrGN in the ARE matrix (refer to the resulting composites here as ARE/PVP-TrGN). It was found that the addition of PVP to the ARE composite material could increase the percolation threshold and dielectric constant of the composite. The results demonstrated that ARE/PVP-TrGN had a percolation threshold of 1.65 wt%, and when the loading of the filler was 1.6 wt%, at 100 Hz, it had a dielectric constant higher than 100, representing a 30 times increase with respect to the neat ARE, and a low dielectric loss of 0.2. In addition, the thermogravimetic (TG) analysis indicated that the composite possessed better thermal stability than that of neat ARE. The elastic modulus of ARE/2% PVP-TrGN was lower than 6 MPa.

Key words: Acrylic Resin Elastomer; Graphene; Thermal Reduction; Permittivity; Percolation

*Jingwen WANG

College of Materials Science and Technology, Nanjing University of Aeronautics & Astronautics, 29 Yudao Street, Nanjing 210016, P. R. China
E-mail: wjw_msc@nuaa.edu.cn

Gaoqiang WANG, Shuwei ZHOU, Senqiang Wu
Department of Materials Science and Engineering, College of Materials Science and Technology, Nanjing University of Aeronautics and Astronautics, Nanjing 211106, P . R. China

Introduction

Recently, growing attention has been paid to high permittivity composite materials for their role in the development of high performance electronic devices, such as supercapacitor, artificial muscle, bio-sensor, intelligent robot, etc.[1] Composite materials with ceramic or polymer as matrix respectively have been extensively researched to achieve high permittivity.[2] However, modern society raises higher and higher claims to materials for its development, and materials that only have single performance can't meet the demand of industry, so only the high dielectric composite material with enhanced comprehensive properties has a wider foreground of applications. Hence, it is of significance to develop dielectric materials with enhanced comprehensive properties.[3] In the existing composite systems, polymeric composites have received more and more attention because of their good processibility, elasticity, high breakdown voltage and superior corrosion resistance.[4]

ARE is a kind of excellent dielectric elastomer, which has the advantages of low elastic modulus, large electric field induced strain and excellent film-forming property compared to other counterparts. Therefore ARE could be a suitable elastomer to use it in MEMS devices and supercapacitors field.[5] In recent years, composites with ARE as matrix have been garnering increasing concern, however, the dielectric constant of ARE is relatively low (< 7). At present, the methods for increasing the dielectric constant of polymer can be classified into three categories: (1) Loading of fillers with high dielectric constant.[6] (2) Introduction of organic dipole groups to the polymer matrix.[7] (3) Addition of conductive fillers. Copper phthalocyanine (CuPc), for instance, a kind of effective high dielectric filler, was commonly used in the first category. As a typical example of the second category, the push-pull dipole N-allyl-N-methyl-p-nitroaniline was grafted onto the poly (dimethyl siloxane) (PDMS) to enhance the dielectric constant of the polymer. In the third category researchers make use of the percolation mechanism of conductive fillers,[8] such as metal powder, carbon nanotubes, carbon black and so on. However, for the first category, only the content of the filler is very large, can dielectric constant become very high. As for the

second category, the polar group will result in an apparent decline in the polymers' breakdown voltage and an increase in humidity sensitivity. By contrast, the third is an efficient way to obtain high dielectric constant while maintaining other excellent performances.

Nanomaterials have been opening a wide window of applications due to their structural features and special properties on a nanometer scale in recent years.[9] As a typical representative, graphene, a two dimensional sheet of sp^2-hybridized carbon, is a new kind of carbon nanomaterial. Since its discovery in 2004, graphene has emerged as a rapidly rising star in the field of material science and has gained tremendous attention due to its extraordinary characteristics, for instance, large aspect ratio, ultrahigh thermal conductivity and electrical conductivity.[10] Thanks to its exceptional physical properties, incorporating a small amount of graphene into the polymer matrix can dramatically enhance the electrical and mechanical properties of the polymer, so polymeric composites filled with graphene have drawn unwavering interest of many researchers.[11] Moreover, compared with zero and one dimensional nanomaterials, graphene has larger aspect ratio, which makes it easier to overlap to form a percolation network. As a result, the nanocomposites with high dielectric constant can be prepared by the loading of less graphene. Thus graphene is regarded as a desirable selection of nanofillers for preparing polymeric nanocomposites with excellent properties.[12]

Nowadays, there have been some methods for fabricating graphene nanosheets, such as micromechanical cleavage of graphite,[13] epitaxial growth method,[14] chemical vapor deposition (CVD), alkali metals intercalation and expansion,[15] chemical and thermal reduction of graphite oxide (GO),[16] and exfoliation of GO.[17] Among them the oxidation-reduction method takes the dominant position, because the method is suitable for large industrial scale production. As for preparing graphene by chemical reduction that involves complicated procedure, hydrazine, sodium hydroxide and so on are commonly selected as reducing agents. However, most of these reducing agents are highly toxic, which will cause pollution to the environment, moreover, the treatment of waste liquid increases the costs of production. By contrast, fabricating

graphene nanosheets by thermal reduction is facile and efficient, more importantly, it is pollution-free. And the thermally reduced graphene is thought to be driven by thermal energy-induced bond cleavage.[18] Therefore, thermal reduction method has become a preferred route .

The electric and mechanical properties of a polymeric nanocomposite with graphene as filler are largely determined by the dispersion property of filler in matrix as well as the adhesion property between filler and matrix.[19] But graphene has high tendency toward agglomerating together via van der Waals attraction because of the special planar sp^2-carbon,[20] which will result in an increase of dielectric loss. Thus the crucial task of obtaining high dielectric constant while maintaining satisfactory dielectric loss is to prevent the agglomeration and overlapping of conductive fillers in the polymer matrix.[21] The strategies to overcome the strong van der Waals forces are divided into two categories: (1) Covalent modification. In this category the graphene was modified by grafting it onto the polymer molecular chain.[22] However, there are no active groups on the graphene molecule. (2) Noncovalent modification. In this category the graphene was modified by using the surface active agent,[23] which can protect the structure of graphite lattice.

In a recent study, PVP, a type of commonly used low-cost, non-toxic and biocompatible surface active agent that has good solubility in water and many organic solvents, was utilized to prevent the aggregation of graphene in solvents,[24] which greatly improved the performance of the composite materials.

In this investigation, a handy strategy was put forward to improve the dielectric properties of ARE. The graphene nanosheets prepared by thermal reduction was added to ARE to form a brand-new dielectric composite system. And PVP was employed as the surface active agent of the graphene nanosheets to improve the dielectric properties of composite, which was also never seen before. The TrGN modified by PVP was blended with ARE, and indeed the composite films obtained by solution casting method exhibited high dielectric constant, low dielectric loss as well as the good flexibility.

Experimental Section

Reagents

Natural graphite, potassium permanganate ($KMnO_4$) and benzoperoxide (BPO) were purchased from American Aladdin Reagent Co., Ltd. Concentrated sulfuric acid (H_2SO_4, 98%), sodium hydroxide (NaOH), concentrated hydrochloric acid (HCl, 33%) and dimethylformamide (DMF) purchased from Nanjing Chemical Reagent Co., Ltd were of analytical grade, and DMF was dried with CaH_2 and distilled in vacuum before use. Hydrogenperoxide (H_2O_2, 30%) was obtained from Sigma-Aldrich, Inc. Distilled water was prepared in laboratory. Styrene (St) and butyl acrylate (BA) purchased from Shanghai Ling Feng Chemical Reagent Co., Ltd were all of analytical grade, and the inhibitors were removed by NaOH solution followed by distillation before use. The analytical grade hydroxyethyl methylacrylate (HEMA) was purchased from American Aladdin Reagent Co., Ltd and purified with activated carbons. PVP was bought from Chinese Medicine Group Chemical Reagent Co., Ltd.

Preparation of TrGN

The preparation process referred to ref 25 and was slightly altered. Detailed route was as follows. Graphite oxide (GO) was synthesized from natural graphite by the method of modified Hummers.[26] The preparation procedure consisted of three steps. (1) At the reaction stage of low temperature, natural graphite powder (2 g) was added into a 0 °C concentrated sulfuric acid solution (46 mL), and homogeneous mixing of natural graphite with concentrated sulfuric acid was achieved by mechanical stirring. Successively, $KMnO_4$ (6 g) was added gradually to the solution for 1 h under stirring, after which the solution was stirred for another 2 h below 5 °C. (2) The container was transferred to a lukewarm bath to keep the temperature of the solution at about 35 °C, and the solution was stirred for 2 h. (3) Distilled water (92 mL) was slowly added to the system to keep the temperature between 90 °C and 100 °C, and the solution was stirred for 1 h. Later, distilled water (280 mL) and H_2O_2 (30%, 20 mL) were slowly added to the solution in succession under stirring, which was followed by 30 min's

stirring, and the color of the solution gradually turned yellow. After that, the crude product was obtained by filtration and 10% dilute hydrochloric acid solution was used to wash the product three times to remove metal ions completely. Then the resulting product was washed thoroughly with distilled water followed by centrifugation until the pH of supernatant was 7. And presently the graphite oxide (GO) was dried at 40 °C for 48 h. At last, the graphite oxide (GO) was put into a tubular furnace and heated from ambient temperature to 900 °C at a heating rate of 5 °C/min under the protection of nitrogen and then maintained for 10 min.

Synthesis of ARE

The ARE here was synthesized via radical polymerization. The synthetic route referred to ref 27 and was made minor modification. The synthesis procedure was as follows. First of all, St (0.35 g), BA (0.60 g) and HEMA (0.05 g) were successively added into a three-necked flask (100 mL) equipped with an Allihn condenser, a magnetic stirrer and a thermometer. Then, DMF (1.5 mL) was also added into the flask as the solvent and BPO (0.005 g) was added as the initiator (BPO here was firstly dissolved into DMF and then the solution was dropped into the flask instead of adding BPO to the flask directly, which was the minor modification that was made). The reaction was carried out at about 100 °C for 5 h under nitrogen protection. Finally, the reaction device was converted into a vacuum distillation unit to remove unreacted monomers and solvent.

Dispersion performance test of TrGN in DMF

Firstly, the solution of PVP was prepared by dissolving 10 mg PVP in 5 mL DMF and stirring for 10 min. Then 10 mg TrGN was added into the solution, which was subjected to ultrasonic treatment for 1 h at room temperature,[28] and the resulting solution was labeled as PVP-TrGN/DMF. As comparison, the DMF dispersion of TrGN without the modification of PVP was fabricated under the same conditions and labeled as TrGN/DMF. At last the two solutions were centrifugated under the same

conditions for 3 min, then they were left overnight.

Preparation of the composite films

The composite films here were fabricated by solution casting method. In a typical experiment, ARE (1 g) was dissolved in DMF under stirring at room temperature, then a desired amount of PVP-TrGN dispersed in DMF by ultrasonic vibration was added to the solution under magnetic stirring. The resulting solution was stirred for 1 h, then the solution was cast onto a polytetrafluoroethylene mold and dried at atmospheric pressure at 80 °C for 8 h. Finally the mixture was dried under vacuum at 80 °C for 8 h to remove DMF completely, thus the nanocomposite film was obtained. The weight percentage of modified TrGN was designed as 0.3%, 0.5%, 0.7%, 1.0%, 1.5%, 1.7%, 2.0%, 4.0%, 7.0%, and the corresponding composite films were marked as ARE/x PVP-TrGN (where x is the weight percentage of filler). For comparison, the blend of ARE and TrGN were prepared under the same conditions, and the composite films were marked as ARE/x TrGN.

Characterization

Raman spectra were recorded with a inVia Raman spectrometer (HORIBA, Kyoto, Japan) with 488 nm diode laser excitation on a 300 lines/mm grating at ambient temperature. X-ray diffraction (XRD) patterns of samples were monitored at room temperature with a XRD-6100 diffractometer (SHIMADZU, Kyoto, Japan) equipped with a Cu Ka radiation source (λ = 1.540 Å.). The scanning range was from 5° to 40° and the scanning interval was 5°. Fourier transform infrared (FTIR) spectra were collected with a Nicolet Nexus-670 spectrometer (Madison, America) by incorporating the sample in a KBr disk. X-ray photoelectron spectra (XPS) were measured with a PHI Quantera Ⅱ spectrometer (Ulvac-Phi, Chigasaki, Japan). Transmission electron microscopy (TEM) imaging was performed with a Tecnai-12 electron microscope (Philips company, Amsterdam, Holland) operating at an accelerating voltage of 120 kV, and the TEM samples were prepared by dispersing a

small amount of dry powder into ethanol followed by ultrasonic vibration and placed onto copper grids before observation. Nuclear magnetic resonance (^{1}H-NMR) spectrum was carried out by a Bruker DRX-500 spectrometer (Bruker, Germany) with chloroform-d as the solvent. The number-average molecular weight of ARE was measured by PL-GPC 200 (Shanghai, China) instrument using standard polyethylene as reference and DMF as solvent at a flow rate of 0.35 mL· min^{-1} operated at 40 °C. The fracture surfaces morphologies of the film samples fractured in liquid nitrogen were observed with a Hitachi S-4800 (Tokyo, Japan) scanning electron microscopy (SEM). The electric resistance measurements were accomplished by a standard four-point probe (kdy-1) produced by Guangzhou Kund Technology Co. Ltd. Dielectric properties were measured by a HP 4294A precision impedance analyzer (Dongguan, China) in the frequency range of 40 Hz to 1 MHz at room temperature and the permittivity values (ε) of the samples were calculated by the following equation:

$$\varepsilon = \frac{Ch}{\varepsilon_0 A} \quad (1)$$

where C is the measured capacitance of the sample (in parallel mode), ε_0 is the vacuum dielectric constant (~ 8.85×10^{-12} F· m^{-1}), A represents the area of the electrode smeared on both sides of the sample before measurement, and h represents the thickness of the sample. The electric breakdown strength was measured by a Dielectric Withstand Voltage Test (Beijing Electromechanical Research Institute, China). Thermogravimetric (TG) analysis curves were obtained by a Simultaneous Thermal Analyzer (STA409PC, NETZSCH company, Bavarian State, Gemany). The TG film samples with the weight of about 10 mg were sealed in aluminium oxide pans and the temperature was set from 25 °C to 600 °C at a rate of 10 °C/min. The elastic performance test of the film samples was operated by a DMTA-V dynamic mechanical thermal analyzer (Rheometric Scientific, Inc.) at room temperature and 1 Hz using a strain dependent mode.

Results and Discussion

Raman spectrum is a widely used tool for characterizing the graphene. As were shown in Figure 1, the Raman spectrum of natural graphite displays a well-known strong G peak (the E_{2g} phonon mode of sp^2 carbon atoms) at 1582 cm^{-1}, a weak D peak (the breathing mode of k-point mode of A_{1g} symmetry) at 1338 cm^{-1}. The generation of D peak caused by defects was due to the existence of the pentagon, heptagon or other local defects. In the Raman spectrum of TrGN, the G peak is broadened and shifted upward to 1598 cm^{-1}, in addition, the strength of G peak decreases. Meanwhile, the strength of D peak at 1338 cm^{-1} increases apparently, which might be due to the significant decrease of the size of the in-plane sp^2 domains because of oxidation and thermal exfoliation, and partially ordered graphite crystal structure of graphene nanosheets. Compared with TrGN, the I_D /I_G ratio (the intensity ratio of the D band relative to the G band) of PVP-TrGN slightly increases, which might indicate that the grain size of graphene continues to decrease and the lattice defects increase due to presence of PVP.

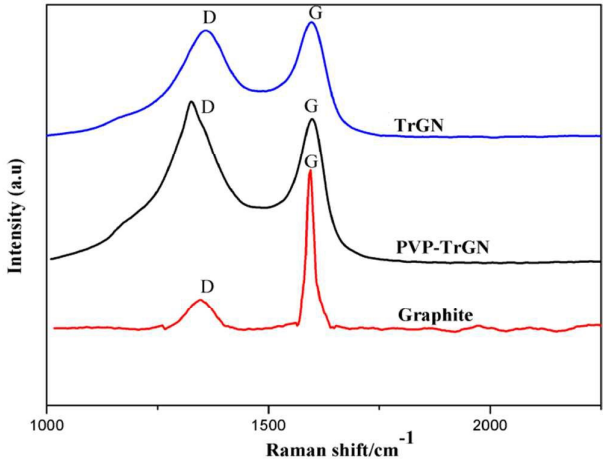

Figure 1 Raman spectra of natural graphite, TrGN and PVP-TrGN

XRD was further utilized to characterize the structures of natural graphite, GO, TrGN and PVP-TrGN. As were presented in Figure 2, the graphite appeared a strong peak at 26.4°, corresponding to (002) lattice planes. As a result of the intercalation of functional groups resulted from graphite oxidation into the interlayers of graphite sheets, GO exhibited a sharp diffraction peak at 9.8° with a wider inter-lamellar

spacing (d-spacing) than graphite. A broad swelling diffraction peak between 20° and 25° was observed in the spectra of TrGN and PVP-TrGN, which was attributed to (002) lattice planes of the graphene. Moreover, very weak characteristic peaks at about 10° were also observed in the spectra of TrGN and PVP-TrGN separately, which indicated that the reduction degree of GO was not completely. Diffraction angle of TrGN was slightly larger than that of PVP-TrGN, which was because lamellar spacing of PVP-TrGN was larger than that of TrGN as a result of adsorption of PVP on graphene nanosheets. FTIR spectra of natural graphite, GO, TrGN and PVP-TrGN (Figure S1 in Supplementary Information) further proved that GO was reduced successfully and PVP was adsorbed on graphene nanosheets effectively. The results were consistent with XRD.

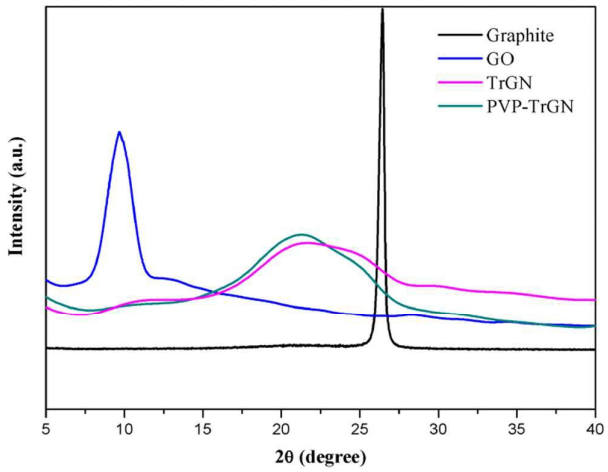

Figure 2 XRD patterns of natural graphite, GO, TrGN and PVP-TrGN

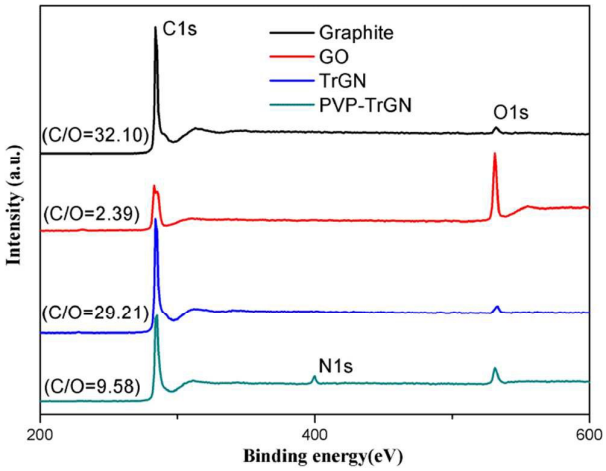

(a)

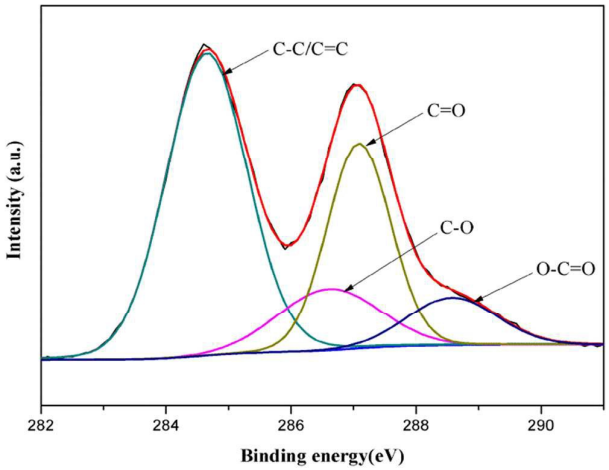

(b)

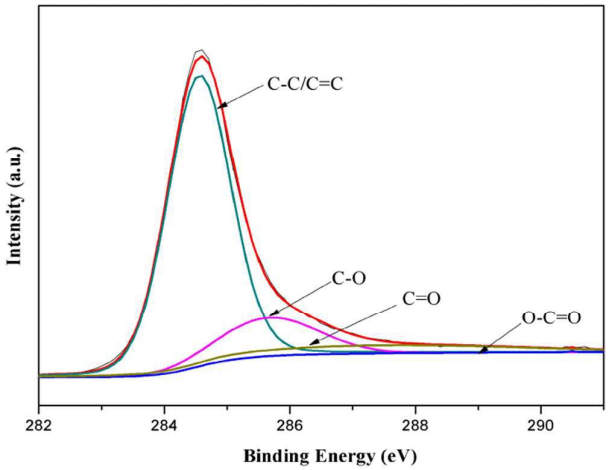

(c)

Figure 3 XPS general spectra of natural graphite, GO, TrGN and PVP-TrGN (Fig 3a) and XPS high-resolution C 1s spectra of GO (Fig 3b) and TrGN (Fig 3c)

Fig 3a showed the XPS general spectra of graphite, GO, TrGN and PVP-TrGN,

and the C/O ratio were 32.10, 2.39, 29.21 and 9.58 respectively. It should be also mentioned that the decline in C/O ratio of GO indicated the introduction of oxygen-containing groups in the oxidation process. And the increase in C/O ratio of TrGN indicated that most of the oxygen-containing groups were removed after thermal reduction at 900 °C. The peak of C-N (286.0 eV) corresponded to the N in the C-N bonds of PVP. XPS high-resolution C 1s spectra of GO and TrGN were shown in Fig 3b and Fig 3c separately. There were four peaks in C1s spectra of GO, the peak at 284.7 eV could be ascribed to C-C/C=C, the other peaks arised from C-O (hydroxyl and epoxy, 286.6 eV), C=O (carbonyl, 287.2 eV) and O-C=O (carboxyl, 288.8 eV) groups separately. After thermal reduction, as was shown in Fig 3c, the oxygen peaks in the C 1s spectra of TrGN were significantly weakened, which indicated that most of the oxygen groups had been removed after reduction.

Digital pictures of PVP-TrGN and TrGN dispersed in DMF with the aid of ultrasonication treatment for 1 h (Figure S2 in Supplementary Information) indicated that PVP can prevent graphene nanosheets from aggregating sterically by being adsorbed on the surface of the graphene, and the resulting dispersion was stable against centrifugation. The explanation for the adsorption mechanism is as follows. The unpaired electrons on the carbonyl group (C=O) and C-N bond of PVP molecules could form strong π–π interaction with electron cloud on the surface of graphene, furthermore, PVP's long chain fully extends to the solvent and forms a thick adsorption layer, resulting in steric hindrance effect that prevents the stacking of graphene layers.[29] Thus graphene in the solvent can obtain better stability and dispersion.

TEM images of TrGN and PVP-TrGN were exhibited in Figure 4. As we can see, due to absence of PVP, TrGN showed obvious aggregation and stacking sheet structure (Fig 4a), by contrast, PVP-TrGN presented fewer layers because of presence of PVP (Fig 4b). This phenomenon further proved the effect of PVP on the stability of graphene.

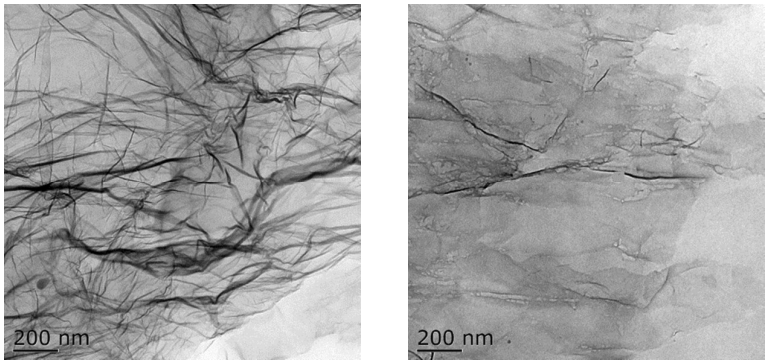

(a) (b)

Figure 4 TEM images of TrGN (Fig 4a) and PVP-TrGN (Fig 4b)

FTIR and 1H-NMR spectra of ARE (Figure S3 and Figure S4 in Supplementary Information) were utilized to characterize the structure. And the spectra showed that ARE was synthetised successfully. In order to further investigate the quality of polymer synthesized, the number-average molecular weight of ARE was measured and the result was 67549 $g \cdot mol^{-1}$.

The dispersion state of filler in the matrix was observed clearly with SEM (Figure S4 in Supplementary Information). Micrographys indicated that TrGN without the modification of PVP tended to aggregate and stack, by contrast, PVP-TrGN exhibited very homogeneous dispersion in the matrix.

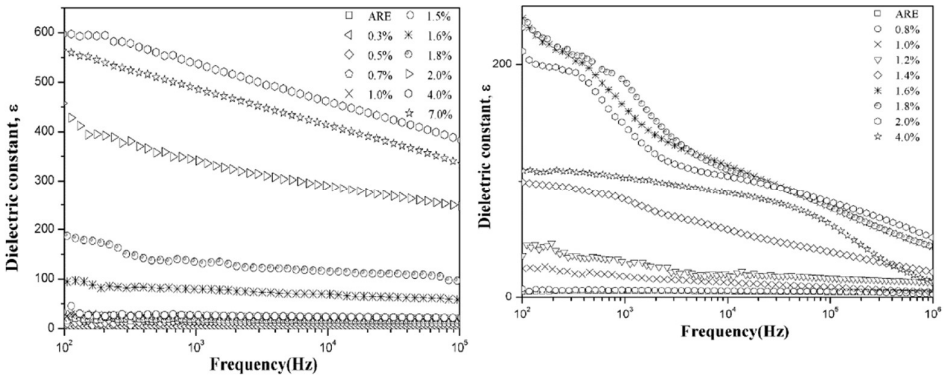

(a) (b)

Figure 5 Dielectric constant of ARE/PVP-TrGN (a) and ARE/ TrGN(b) with different weight fractions of filler measured at room temperature as a function of frequency

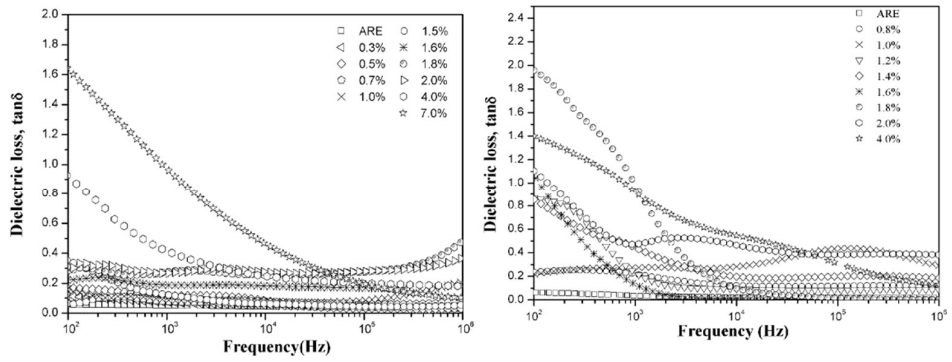

(a) (b)

Figure 6 Dielectric loss of ARE/PVP-TrGN (a) and ARE/TrGN (b) with different weight fractions of filler measured at room temperature as a function of frequency

The frequency dependence of dielectric constant and dielectric loss of ARE/PVP-TrGN composites were depicted in Fig 5a and Fig 6a respectively. As was demonstrated in Fig 5a, when the content of the filler was low, the dielectric constant varied little with frequency, showing a nearly constant of permittivity. When the content of the filler reached a critical value, the dielectric constant decreased with increasing frequency. The explanation for this phenomenon is as follows. Certain polarization produced by the orientation arrangement of some dipoles can contributed to formation of dielectric constant. Due to the variation of frequency, the dipoles reverse with the change of the external electric field, when the frequency turns high, the inversion of dipoles can't keep up with the electric speed because of the internal resistance of the material.[30] Under the condition of high frequency, some dipoles stop inversion, which results in disappearing of contributions to dielectric constant. The almost frequency independence of dielectric constant when the content of filler was low indicated that there was no plentiful accumulation of interfacial charges inside the nanocomposites. The variation tendency of dielectric loss with frequency was also represented in Fig 6a. Generally speaking, the variation of dielectric loss with frequency was consistent with the variation of dielectric constant. As comparison, the frequency dependence of dielectric constant and dielectric loss of ARE/TrGN

composites were depicted in Fig 5b and Fig 6b respectively.

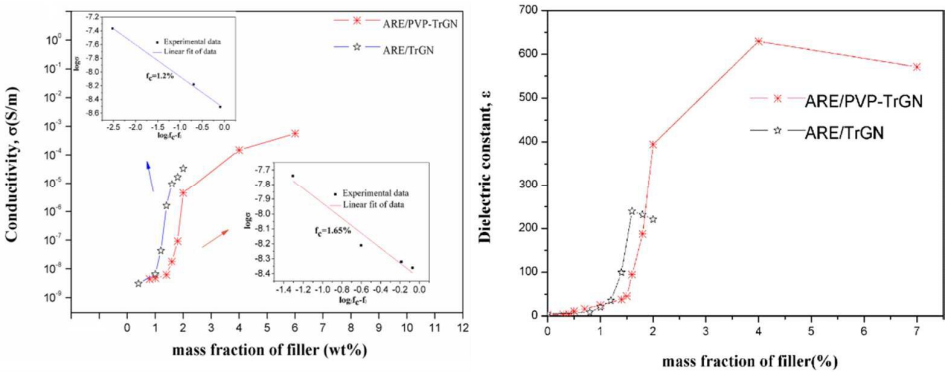

(a) (b)

Figure 7 DC conductivity of ARE/PVP-TrGN and ARE/TrGN nanocomposites as a function of the filler content measured at room temperature (a) and Dielectric constant of ARE/PVP-TrGN and ARE/TrGN nanocomposites as a function of the filler content measured at 100 Hz and room temperature (b).

The content dependence of DC conductivity and dielectric constant (at 100 Hz) of ARE/PVP-TrGN composites were demonstrated in Fig 7a and Fig 7b respectively. Generally speaking, the dielectric constant of the composites increased with the growing loading of the filler. The increase in dielectric constant is attributed to two reasons: (1) The Maxwell–Wagner–Sillars (MWS) polarization, which is related to the entrapment of nomadic charges between the insulator and conductor interface,[31] that is, the interfacial polarization. MWS polarization will occur as long as the charge carriers at an interface between matrix and filler accumulates. For the composite mentioned above, the charges in conductive TrGN were easily delocalized, which accumulated at the interface of TrGN and ARE insulator layer when they were driven by the applied electric field, and the accumulation of the charges contributed to a large polarization. With the increasing of filler content, MWS polarization was significantly improved. As a result, dielectric constant of the composite was enhanced quickly. (2) The formation of "microcapacitors" in ARE matrix, that is, two paralleled graphene sheets are isolated by a thin insulating ARE interlayer.[32] In addition, it was also interesting to observe the figures in detail. As were demonstrated in Fig 7a and Fig 7b, when the content of filler was low, direct current (DC) conductivity and dielectric

constant increased slowly with the increasing of the filler content. When the content reached a critical value, there was a huge increase in the DC conductivity and dielectric constant. The phenomena obviously indicated that the transition from insulator to conductor occurred in the ARE/PVP-TrGN composites. The following interpretative statement was made to explain above transition. The dielectric constant of the composite could be improved by adding a small amount of graphene to the polymer matrix, which was because conductive graphene with two-dimensional structure and insulating polymer could constitute microcapacitors and these microcapacitors improved the charge storage ability of the composite. When the content of graphene was low, there was few microcapacitors, so the DC conductivity and dielectric constant showed slight increase. With the increasing of the filler content, there were more and more microcapacitors, and the DC conductivity and dielectric constant of the composite continued to increase. These two dimensional nanomaterials mutually overlapped in the polymer matrix and gradually built up a conductive network. When the content of graphene was beyond a critical value, the conductive network happened to be able to form, and the transition of the composite from insulator to conductor was realized, which resulted in a significant increase of the DC conductivity and dielectric constant. This phenomenon was called percolation, and the critical value was called percolation threshold. The percolation threshold of composites can be deduced from the following power laws:[33]

$$\sigma_{dc} \propto (p_c - p)^t \qquad \text{for } p<p_c \qquad (2)$$

where σ_{dc} is the DC conductivity of composites; p_c is the percolation threshold and p is the fraction of the conductive filler; t is a scaling constant. By fitting the DC conductivity figures for $p<p_c$, as was presented in inset of Fig 7a, a percolation threshold value of 1.65 wt% was obtained. As was shown in Fig 7b, the dielectric constant increased remarkably and reached to more than 180 when the loading of filler was 1.8 wt%, which was about 60 times larger than that of neat ARE (~ 3.2). As comparison, The content dependence of DC conductivity and dielectric constant of ARE/TrGN composites were also shown in Fig 7a and Fig 7b respectively. The percolation threshold of 1.20 wt% was obtained by the same method.

Compared with ARE/TrGN composite, ARE/PVP-TrGN composite had higher dielectric constant and percolation threshold, which was because the addition of PVP improved the dispersion performance of graphene in the matrix. And then the improved dispersion delayed the formation of conductive network of filler in the matrix, which helped to the production of more microcapacitors, and these microcapacitors in turn contributed to higher dielectric constant. At the same time, the latency of the formation of conductive network of filler directly raised the percolation threshold.

The electric breakdown strength of ARE/1.0% PVP-TrGN and ARE/1.0% TrGN was measured by a Dielectric Withstand Voltage Test separately. The facts showed that the electric breakdown strength of ARE/1.0% PVP-TrGN (45 V/μm) was higher than that of ARE/1.0% TrGN (37 V/μm), which was because TrGN had a poor dispersion in the matrix and was easier to form a conductive network.

TG curves for neat ARE and ARE/PVP-TrGN composites (Figure S5 in Supplementary Information) were utilized to investigate the thermal stability of the composites. The TG results indicated that the thermal degradation temperature of neat ARE was about 367 °C, and the thermal degradation temperature of ARE/PVP-TrGN composite was higher than that of neat ARE. Moreover, the thermal degradation temperature of ARE/PVP-TrGN composite increased with the increasing of the filler content. The curves also demonstrated that the addition of the filler could slow down the weight loss during thermal degradation. The TG curve of ARE/2 wt% PVP-TrGN composite showed the amount of weight residue increased by 6.2% in comparison with neat ARE at 600 °C. These phenomena can be explained as follows. PVP has a long nonpolar polyethylene chain, which has a good adsorption effect upon thermally reduced graphene nanosheets. Moreover, because the polymer that we synthesized has high viscosity, there is an interaction between PVP-TrGN and ARE inevitably, which reduces the thermal amplitude of the molecular chains. So the thermally unstable groups of ARE were transformed into more stable structures, which contributed to reduction of the possibility of thermal degradation.

DSC curves of neat ARE and ARE/PVP-TrGN composites (Figure S6 in

Supplementary Information) showed that the decomposition enthalpy of neat ARE was about 206.8 J/g, and the decomposition enthalpy of the composites with the filler content of 0.5%, 1.5%, 2.0% were about 236.9 J/g, 252.6 J/g, 256.4 J/g respectively. Removing the weight of TrGN, the decomposition enthalpy of neat AE were about 238.1 J/g, 256.4 J/g, 261.6 J/g respectively, which further proved that the addition of graphene improved the thermal stability of the composite.

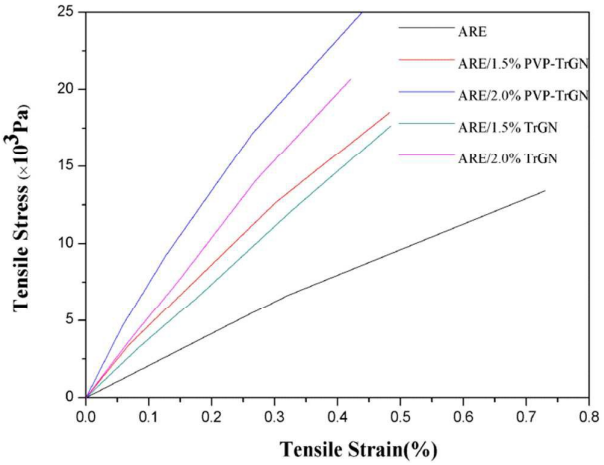

Fig 8 Elastic deformation stage of stress-strain curves of neat ARE, ARE/PVP-TrGN and ARE/TrGN nanocomposites

The elastic deformation stage of representative stress-strain curves of the ARE/PVP-TrGN and ARE/TrGN nanocomposites were depicted in Fig 8. As we can see, the addition of PVP-TrGN and TrGN increased the initial modulus of the polymer (1.19 MPa). Moreover, PVP-TrGN showed a better reinforcement effect than that of ARE/TrGN, which might be because presence of PVP increased the dispersion property of filler in matrix. Large surface area of graphene nanosheets was in contact with ARE matrix and the better interfacial interaction leaded to an efficient load transfer from ARE matrix to graphene nanosheets, contributing to a increase of the mechanical properties of nanocomposites. However, no matter what kind of composite, the elastic modulus of the composites was not very large and could still be accepted in the practical application. Therefore, the preparation of this kind of composite material was of practical significance.

Conclusion

In summary, ARE was synthesized by free radical polymerization. Graphene nanosheets were prepared by chemical oxidation of nature graphite followed by thermal exfoliation and reduction of GO. Dielectric elastomer composites, ARE/PVP-TrGN and ARE/TrGN have been prepared by using solution casting method. Compared with ARE/TrGN, ARE/PVP-TrGN composite not only possessed better dielectric properties, but also had enhanced thermal stability and elasticity because of the improved dispersion property of filler. The ARE/PVP-TrGN composite with the filler content of 1.6% had a dielectric constant higher than 100 and a dielectric loss of 0.2, meanwhile, it also had an elastic modulus lower than 6 MPa at room temperature. However, PVP's ability to enhance the dispersion of graphene in solvents is limited. Further property improvement can be expected through the amelioration in the composite fabrication process, especially by grafting the graphene oxide onto the acrylic resin to increase the distribution uniformity of the filler in polymer matrix.

Acknowledgments

This work was supported by the National Natural Science Foundation of China (No. 21174063), the Natural Science Foundation of Jiangsu Province (No. BK20131358), the Aeronautical Science Foundation of China (No. 2011ZF52063 and No. 2014ZF52069), and A Project Funded by the Priority Academic Program Development of Jiangsu Higher Education Institutions (PAPD).

References

1 J. H. Yu, X. Y. Huang, C Wu and P. K. Jiang, Dielectrics and Electrical Insulation, IEEE Transactions on, 2011, 18, 478-484.

2 E. Lee and Y. G. Jeong, Fibers and Polymers, 2015, 16, 2021-2027.

3 X. Y. Huang, P. K. Jiang and L. Y. Xie, Applied Physics Letters, 2009, 95, 2901-2903

4 Z. M. Dang, J. K. Yuan, J. W. Zha, T. Zhou, S. T. Li and G. H. Hu, Progress in Materials Science, 2012, 57, 660-723.

5 Q. M. Zhang, H. F. Li, Poh M, F. Xia, Z. -Y. Cheng, H. S. Xu and C Huang, Nature, 2002, 419, 284-287.

6 K. S. Lam, Y. Zhou, Y. W. Wong and F. G. Shin, Journal of applied physics, 2005, DOI: 10.1063/1.1906285

7 B. Kussmaul, S. Risse, G. Kofod, R. Wache, M. Wegener, D. N. McCarthy, H. Kruger, R. Gerhard, Advanced Functional Materials, 2011, 21, 4589-4594.

8 S. Zhang, N. Zhang, C. Huang, K. Ren and Q.M. Zhang, Advanced Materials, 2005, 17, 1897-1901.

9 H.K. F. Cheng, N. G. Sahoo, Y. P. Tan, Y. Z. Pan, H. Q. Bao, L. Li, S. H. Chan and J. H. Zhao, ACS applied materials & interfaces, 2012, 4, 2387-2394.

10 A. K. Geim and K. S. Novoselov, Nat Mater, 2007, 6, 183-191.

11 C. Soldano, A. Mahmood and E. Dujardin, Carbon, 2010, 48, 2127-2150.

12 R. Sengupta, M. Bhattacharya, S. Bandyopadhyay and A. K. Bhowmick, Progress in polymer science,2011, 36, 638-670.

13 K. S. Novoselov, A. K. Geim, S. V. Morozov, D. Jiang, Y. Zhang, S. V. Dubonos, I. V. Grigorieva, A. A. Firsov, science, 2004, 306, 666-669.

14 A. N. Obraztsov, Nature nanotechnology, 2009, 4, 212-213.

15 F. T. Thema, M. J. Moloto, E. D. Dikio, N. N. Nyangiwe, L. Kotsedi, M. Maaza, and M. Khenfouch, Journal of chemistry, 2012, DOI: 10.1155/2012/150536

16 X. Liu, L. Yi, X. Wang, J. Su, Y Song and J Liu, international journal of hydrogen energy, 2012, 37, 17984-17991.

17 G. Moula, M. A. Mumin and P. A. Charpentier, J. Nanomater. Mol. Nanotechnol, 2013, DOI: 10.4172/2324-8777. S1-002.

18 Kalaitzidou, Kyriaki, Exfoliated graphite nanoplates as reinforcement for multifunctional polypropylene nanocomposites, Michigan State University, Michigan State, 2006.

19 H. Wang, P. G. Ren, J. Z. Xu, D. X. Yan, Z. M. Li and L. Xu, Composite Interfaces, 2014, 21, 203-215.

20 N. Ruecha, R. Rangkupan, N. Rodthongkum and O. Chailapakul, Biosensors and Bioelectronics, 2014, 52, 13-19.

21 P. Xu, H. G. Gui, X. X. Wang, Y. D. Hu and Y. S. Ding, Composites Science and Technology, 2015, 117, 282-288.

22 F. Wen, Z. Xu, S. B. Tan, W. M. Xia, X. Y. Wei and Z. C. Zhang, ACS applied materials & interfaces, 2013, 5, 9411-9420.

23 M. Saha, P. Tambe, S. Pal, P. Kubade, G. Manivasagam, M. A. Xavior and V. Umashankar, Composite Interfaces, 2015, 22, 611-627.

24 S. Liu, X. R. Xing, J. H. Yu, W. J. Lian, J. Li, M. Cui and J. D. Huang, Biosensors and Bioelectronics, 2012, 36, 186-191.

25 H. L. Chen, C. W. Huang, W. Yu and C. X. Zhou, Polymer, 2013, 54, 1603-1611.

26 F. Yavari, H. R. Fard, K. Pashayi, M. A. Rafiee, A. Zamiri, Z. Z. Yu, R. Ozisik, T. B-Tasciuc and N. Koratkar, The Journal of Physical Chemistry C, 2011,115, 8753-8758.

27 R. N. Liu, J. W. Wang, Q. Li, S. Q. Li, S. Zhang and X. J. Ding, Journal of Applied Polymer Science, 2014, 131, DOI: 10.1002/app.39975

28 A. S. Wajid, S. Das, F. Irin, H. S. T. Ahmed, J. L. Shelburne, D. Parviz, R. J. Fullerton, A. F. Jankowshi, R. C. Hedden and M. J. Green, Carbon, 2012, 50, 526-534.

29 Bourlinos AB, Georgakilas V, Zboril R et al (2009) Aqueous-phase exfoliation of graphite in the presence of polyvinylpyrrolidone for the production of water-soluble graphenes. Solid State Commun 149:2172–2176

30 B. K. Dash, P. G. R. Achary and N. C. Nayak, Journal of Materials Science:

Materials in Electronics, 2015, 26, 7244-7254.

31 Q. Su, S. Pang, V. Alijani, C. Li and X. Feng, Advanced materials, 2009, 21, 3191-3195.

32 P. Fan, L. Wang, J. T. Yang, F. Chen and M. Q. Zhong, Nanotechnology, 2012, DOI: 10.1088/0957-4484/23/36/365702

33 Z. M. Dang, Y. H. Lin and C. W. Nan, Advanced Materials, 2003, 15, 1625-1629.